

Quantum-enhanced electrometer based on microwave-dressed Rydberg atoms


Shuhe Wu^{1,2}, Dong Zhang^{1,2}, Zhengchun Li^{1,2}, Minwei Shi^{1,2}, Peiyu Yang^{1,2}, Jinxian Guo^{1,2},
Wei Du^{1,2,*}, Guzhi Bao^{1,2,†} and Weiping Zhang^{1,2,3,4,‡}

¹*School of Physics and Astronomy and Tsung-Dao Lee Institute, Shanghai Jiao Tong University, Shanghai 200240, China*

²*Shanghai Branch, Hefei National Laboratory, Shanghai 201315, China*

³*Collaborative Innovation Center of Extreme Optics, Shanxi University, Taiyuan, Shanxi 030006, China*

⁴*Shanghai Research Center for Quantum Sciences, Shanghai 201315, China*

 (Received 27 April 2023; revised 15 October 2023; accepted 14 November 2023; published 15 December 2023)

Rydberg atoms have shown remarkable performance in sensing microwave fields. The sensitivity of such an electrometer based on optical readout of the atomic ensemble has been demonstrated to approach the photon-shot-noise limit. However, the sensitivity cannot be promoted infinitely by increasing the power of the probe light due to the increased collision rates and power broadening. Compared with classical light, the use of quantum light may lead to a better sensitivity with a lower number of photons. In this paper, we exploit entanglement in a microwave-dressed Rydberg electrometer to suppress the fluctuation of noise. The results show a sensitivity enhancement that beats the shot-noise limit in both cold- and hot-atom schemes. Through optimizing the transmission of the optical readout, our quantum advantage can be maintained with differing absorptive indexes of the atomic vapor, which makes it possible to apply a quantum light source in the absorptive electrometer.

DOI: [10.1103/PhysRevApplied.20.064028](https://doi.org/10.1103/PhysRevApplied.20.064028)

I. INTRODUCTION

The ultrasensitive detection of electric fields plays a significant role in widespread applications, including communications [1,2], remote sensing [3,4], and medical diagnosis [5–7]. Rydberg-atom-based electrometers (RAEs) [8–11], in which the spectroscopic characterizations of atoms are engineered by the optical and electric fields in the process of electromagnetically induced transparency (EIT) [12] and Autler-Townes (AT) splitting [13], bring about a direct International System of Units (SI) traceable and self-calibrated measurement of the electrical amplitude with a broadly dynamic range. These instruments can be very sensitive to electric fields due to the large transition electric dipole moment [14], which leads to a strong atomic response to electric fields. The strength of the signal can be calculated from observing the distance between the two separate peaks caused by the electric field [8,9,15].

When the electric field is strong enough, the splitting can be distinguished in the area called the AT regime. However, precisely measuring the splitting will be hard when the electric field is too small to depart from the AT regime

[8,15]. Under these circumstances, the strength of the electric field can be monitored by observing the variation of the probe transmission instead of the splitting. Recently, photon shot noise (PSN) in the signal readout has been regarded as the main limiting factor to the performance of RAEs [16,17]. The PSN of the probe light and the slope of the readout signal will jointly limit the sensitivity, which can be determined by [18,19]

$$\delta E_{\text{MW}} \equiv \frac{\sqrt{\langle \delta^2 \hat{I} \rangle}}{|\partial \langle \hat{I} \rangle / \partial \epsilon|} \times \frac{1}{|\partial \epsilon / \partial E_{\text{MW}}|}. \quad (1)$$

Here, \hat{I} is the intensity of the detected field, while ϵ and E_{MW} represent the absorptive index and the amplitude of the microwave field, respectively. It is clear that the PSN scales with the square root of the optical power and that the slope of the readout signal is proportional to the optical power, so classically optimized sensors can typically be improved by increasing the laser power. However, the laser-induced collision rates and power broadening [16] will lead to a decrease of the signal slope, which also limits the laser power. In this scenario, squeezed light holds particular appeal for applications due to its ability to further enhance the sensitivity by reducing the PSN with limited laser power, which has been shown in a number of applications [20–24].

*wdsjtu2021@sjtu.edu.cn

†guzhibao@sjtu.edu.cn

‡wpz@sjtu.edu.cn

In this paper, we study absorptive measurement using a beam splitter (BS) to mimic the loss in differential detection and theoretically analyze the characteristics of different schemes, e.g., with coherent and squeezed input states. We then replace the BS with microwave-dressed Rydberg atoms and study the entanglement-assisted microwave electrometer. Since quantum light is extremely fragile to loss, it is necessary to find an operating point that simultaneously maintains a relatively high transmittance of probe light and slope of the observable. We demonstrate that the variation of the electric field E_{MW} affects the transmittance factor ϵ of the probe light and the slope of the observable synchronously; therefore, the minimal observable is realized by operating at the optimal slope and noise through engineering the dressed microwave (MW) field and the light field.

II. SENSITIVITY OF ABSORPTIVE MEASUREMENT

A. Sensitivity with classical field

Before introducing entanglement-assisted RAEs, we start by briefly calculating the sensitivity of absorptive measurement when coherent light and squeezed light are employed, respectively. When the coherent state is employed, absorptive measurement can be achieved by a topology of differential detection as shown in Fig. 1(a). A coherent state \hat{a}_0 is split into \hat{a}_{in} and \hat{b}_{in} by the variable beam splitter (VBS), with a transmissivity of T and a reflectivity of R . \hat{a}_{in} acts as the probe light propagating through a fictitious BS mimicking the absorptive signal of the optical field with the transmission $e^{-\epsilon}$ and \hat{a}_v is the vacuum field induced by the absorptive measurement, while the beam \hat{b}_{in} serves as a reference. The input-output relations of the coherent state scheme are given by

$$\hat{a}_{\text{out}} = \sqrt{Te^{-2\epsilon}}\hat{a}_0 + \sqrt{Re^{-2\epsilon}}\hat{b}_0 + \sqrt{1 - e^{-2\epsilon}}\hat{a}_v, \quad (2)$$

$$\hat{b}_{\text{out}} = \hat{b}_{\text{in}} = \sqrt{T}\hat{b}_0 - \sqrt{R}\hat{a}_0, \quad (3)$$

where T and R are the transmissivity and reflectivity of the VBS with the condition $T + R = 1$. The observable here is defined as

$$\hat{I} = \hat{a}_{\text{out}}^\dagger \hat{a}_{\text{out}} - \hat{b}_{\text{out}}^\dagger \hat{b}_{\text{out}}. \quad (4)$$

We then obtain the slope and noise of the observable,

$$\frac{\partial \langle \hat{I}_c \rangle}{\partial \epsilon} = -2e^{-2\epsilon} I_{\text{si}}, \quad \langle \delta^2 \hat{I}_c \rangle = [e^{-2\epsilon} + \frac{R}{T}] I_{\text{si}}, \quad (5)$$

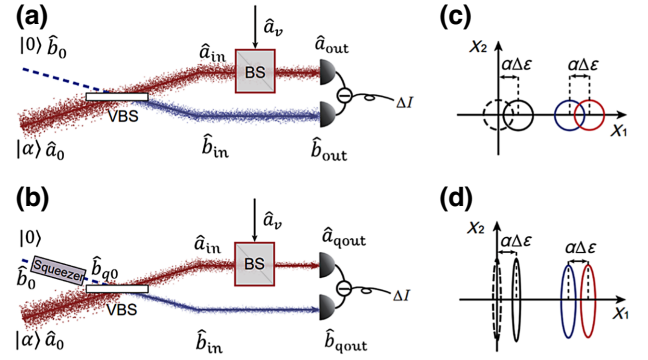


FIG. 1. A schematic diagram for absorptive measurements with (a) classical light and (b) squeezed light, where $|0\rangle$ represents the vacuum state and $|\alpha\rangle$ represents the coherent state; \hat{a}_v is the vacuum field induced by the absorptive measurement. BS, beam splitter; VBS, variable beam splitter. (c),(d) The phase-space ($X_1 - X_2$) representation of the quantum state of the schematic diagrams shown in (a) and (b), respectively. The red and blue circles (ellipses) represent the quantum states of \hat{a}_{out} (\hat{a}_{qout}) and \hat{b}_{out} (\hat{b}_{qout}), respectively. The black circle (ellipse) is the quantum state after the differential detection, with $X_1 = X_{\hat{a}_{\text{out}}}(\hat{a}_{\text{qout}}) - X_{\hat{b}_{\text{out}}}(\hat{b}_{\text{qout}})$ and $X_2 = P_{\hat{a}_{\text{out}}}(\hat{a}_{\text{qout}}) - P_{\hat{b}_{\text{out}}}(\hat{b}_{\text{qout}})$. Here, $X_\beta = \beta + \beta^\dagger$ and $P_\beta = i(\beta^\dagger - \beta)$, with $\beta \in [\hat{a}_{\text{out}}, \hat{a}_{\text{qout}}, \hat{b}_{\text{out}}, \hat{b}_{\text{qout}}]$.

where $I_{\text{si}} = T\alpha^2$ denotes the sensing intensity of the absorptive measurement. According to Eq. (1), the sensitivity can be expressed as

$$\delta_c \epsilon = \frac{\sqrt{\langle \delta^2 \hat{I}_c \rangle}}{|\partial \langle \hat{I}_c \rangle / \partial \epsilon|} = \sqrt{\frac{1}{2} + \frac{R}{2e^{-2\epsilon} T}} \frac{1}{\sqrt{e^{-2\epsilon} I_{\text{si}}}}. \quad (6)$$

The optimum sensitivity can be achieved when $T = 1$ and $R = 0$, which represents a direct detection scheme in which all of the coherent state is transmitted to sense the signal. We then obtain the minimum measurable

$$\delta_c \epsilon = \frac{1}{\sqrt{2} \sqrt{e^{-2\epsilon} I_{\text{si}}}}. \quad (7)$$

For practical applications, the technical noise from the laser also limits the sensitivity [16]. A differential measurement, which is commonly used in precision measurement, can be realized with $e^{-2\epsilon} T = R$, where the excess noise involved in the laser can be cancelled. From Eq. (7), we find that the sensitivity is restricted by the absorption-induced loss and slope and that the fundamental limitation is still PSN originating from the statistical distribution of the photons.

B. Sensitivity with quantum field

We now focus on analyzing the performance of squeezed light in an absorptive measurement. As is well

known, squeezed light is difficult to generate with a large photon flux and is extremely sensitive to loss in an absorptive measurement. We propose a topology similar to homodyne detection, in which the sensing intensity can be boosted by introducing a local oscillator (LO). The optimum operation condition will be studied to realize the maximized sensitivity with a precision that beats the shot-noise limit (SNL).

As shown in Fig. 1(b), we employ a squeezed vacuum state at the unused port of the VBS to replace the vacuum. The input-output relation of the squeezer can be expressed as

$$\hat{b}_{q0} = \cosh r \hat{b}_0 + \sinh r \hat{b}_0^\dagger e^{i\theta}, \quad (8)$$

where \hat{b}_0 is the vacuum state, $\cosh r$ and $\sinh r$ are the gain factors satisfying $\cosh^2 r - \sinh^2 r = 1$, r is the squeezing factor, and θ is the phase of the squeezer. The squeezed light is combined with another much stronger LO field at the VBS to boost the sensing power, since it is exceedingly hard to prepare it with a large photon number. For the squeezed-light scheme, the input-output relationship becomes

$$\hat{a}_{\text{qout}} = \sqrt{e^{-2\epsilon} T} \hat{a}_0 + \sqrt{e^{-2\epsilon} R} \hat{b}_{q0} + \sqrt{1 - e^{-2\epsilon}} \hat{a}_v, \quad (9)$$

$$\hat{b}_{\text{qout}} = \hat{b}_{\text{in}} = \sqrt{T} \hat{b}_{q0} - \sqrt{R} \hat{a}_0. \quad (10)$$

The mode of the LO can be classically represented by $|\alpha\rangle$ due to the much stronger power compared to squeezed vacuum state. We then have the differential intensity between the two detectors:

$$\begin{aligned} \hat{I}_q &= \hat{a}_{\text{qout}}^\dagger \hat{a}_{\text{qout}} - \hat{b}_{\text{qout}}^\dagger \hat{b}_{\text{qout}} \\ &= \alpha \left[(1 + e^{-2\epsilon}) \sqrt{TR} \hat{X}_{b_{q0}} + \sqrt{Te^{-2\epsilon}(1 - e^{-2\epsilon})} \hat{X}_{a_v} \right] \\ &\quad + \alpha^2 (e^{-2\epsilon} T - R). \end{aligned} \quad (11)$$

Here, $\hat{X}_o = \hat{o} + \hat{o}^\dagger$ with $o \in [b_{q0}, a_v]$ is the amplitude quadrature of the optical modes. Note that the intensity term $\alpha^2 (e^{-2\epsilon} T - R)$ can be cancelled when satisfying the condition $e^{-2\epsilon} T = R$. We then give the slope and noise as

$$\frac{\partial \langle \hat{I}_q \rangle}{\partial \epsilon} = -2e^{-2\epsilon} I_{\text{si}}, \quad (12)$$

$$\langle \delta^2 \hat{I}_q \rangle = \left[\frac{1 + e^{-2\epsilon}}{e^{2r}} + 1 - e^{-2\epsilon} \right] e^{-2\epsilon} I_{\text{si}}, \quad (13)$$

where $I_{\text{si}} = T\alpha^2 = \alpha^2 / (e^{-2\epsilon} + 1)$ represents the sensing intensity. According to Eq. (1), we give the

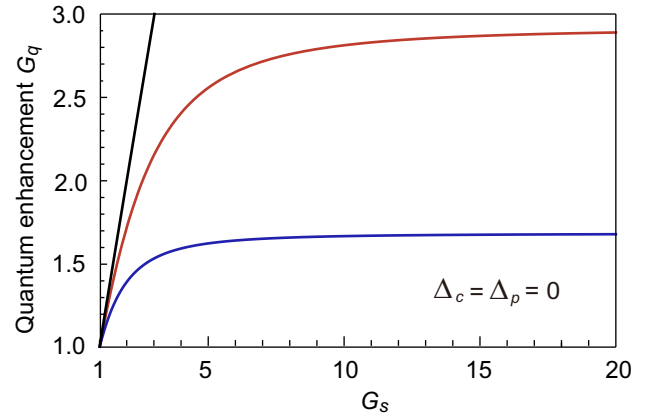


FIG. 2. The quantum enhancement G_q : black line, without absorption; red line, with 10% absorption; blue line, with 50% absorption. The absorption parameters set here correspond to the optimal sensitivity of squeezed-light injection with $\Delta_c = \Delta_p = 0$ (see details in Sec. III). Here, we have labeled the improvement factor $G_s = e^r = \cosh r + \sinh r$.

quantum-enhanced sensitivity of absorptive measurement as

$$\delta_q \epsilon = \frac{\sqrt{\langle \delta^2 \hat{I}_q \rangle}}{|\partial \langle \hat{I}_q \rangle / \partial \epsilon|} = \sqrt{\frac{1 + e^{-2\epsilon}}{e^{2r}} + 1 - e^{-2\epsilon}} \frac{1}{\sqrt{2e^{-2\epsilon} I_{\text{si}}}}. \quad (14)$$

Compared to classical light with differential detection, we find that the sensitivity is improved with a factor of

$$G_q = \frac{\delta_c \epsilon}{\delta_q \epsilon} = \frac{\sqrt{2}}{\sqrt{\frac{1 + e^{-2\epsilon}}{e^{2r}} + 1 - e^{-2\epsilon}}}. \quad (15)$$

This improvement is same as the noise reduction originating from the squeezed-light injection. The quantum enhancement is maximal when the absorption is very small ($\epsilon \rightarrow 0$), indicating an improvement factor of $G_s = e^r$.

Next, we further analyze the influence of G_s on the quantum enhancement G_q with $\Delta_c = \Delta_p = 0$, which is given in Fig. 2. The black line shows the quantum enhancement G_q without absorption, which is proportional to G_s . The quantum enhancement G_q with 10% and 50% absorption are shown with the red and blue lines, respectively. The absorption parameters set here correspond to the optimal sensitivity of squeezed-light injection in the case of cold and hot atoms (see details in Sec. III). It is noted that with the increase of G_s , the quantum enhancement G_q in both cases tends to be saturated due to the existence of absorption. Based on this, we choose $r = 2.5$ to measure the sensitivity.

III. PRINCIPLE OF QUANTUM NOISE-LIMITED ELECTROMETER

In this theory, the RAEs are achieved by cesium (Cs) atomic vapor with a four-level ladder structure, as shown in Fig. 3(a). The frequencies of transition from $|1\rangle$ to $|2\rangle$ and from $|2\rangle$ to $|3\rangle$ are labeled as ω_{21} and ω_{32} , with resonance frequencies of 780 nm and 480 nm, respectively. A weak probe light field with a frequency of ω_p and a strong coupling light field with a frequency of ω_c interact to each transition with a frequency near atomic resonance and the quantum interference from the two excitation pathways produces a dark state that creates a transparent window for the probe light field, termed EIT.

A MW field with a frequency of ω_{MW} nearby Rydberg transition $|3\rangle$ to $|4\rangle$ will reduce the transmitted intensity of the probe light, which is the physical quantity used to estimate the strength of the electric field in our strategy. The Hamiltonian of the system after use of the rotating-wave approximation can be written as

$$\hat{H} = \hbar \begin{bmatrix} 0 & \xi^* \hat{a}^\dagger & 0 & 0 \\ \xi \hat{a} & \Delta_p & \frac{\Omega_c^*}{2} & 0 \\ 0 & \frac{\Omega_c}{2} & \Delta_c + \Delta_p & \frac{\Omega_{MW}^*}{2} \\ 0 & 0 & \frac{\Omega_{MW}}{2} & \Delta_{MW} + \Delta_c + \Delta_p \end{bmatrix}, \quad (16)$$

$$D_{\mu\nu} = \begin{bmatrix} \gamma_2 \sigma_{22} + \gamma_3 \sigma_{33} + \gamma_4 \sigma_{44} & -\frac{\gamma_2}{2} \sigma_{12} & -\frac{\gamma_3}{2} \sigma_{13} & -\frac{\gamma_4}{2} \sigma_{14} \\ -\frac{\gamma_2}{2} \sigma_{12} & -\gamma_2 \sigma_{22} & -\frac{\gamma_2 + \gamma_3}{2} \sigma_{23} & -\frac{\gamma_2 + \gamma_4}{2} \sigma_{24} \\ -\frac{\gamma_3}{2} \sigma_{31} & -\frac{(\gamma_2 + \gamma_3)}{2} \sigma_{32} & -\gamma_3 \sigma_{33} & -\frac{(\gamma_3 + \gamma_4)}{2} \sigma_{34} \\ -\frac{\gamma_4}{2} \sigma_{41} & -\frac{(\gamma_2 + \gamma_4)}{2} \sigma_{42} & -\frac{(\gamma_3 + \gamma_4)}{2} \sigma_{43} & -\gamma_4 \sigma_{44} \end{bmatrix}, \quad (18)$$

in which γ_i is the spontaneous decay from the states $|i\rangle$ to $|i-1\rangle$ and $\hat{F}_{\mu\nu}$ is the Langevin atomic force.

The differential equation describing the propagation and temporal evolution of the quantum field operator is

$$\left(\frac{\partial}{\partial t} + c \frac{\partial}{\partial z} \right) \hat{a}(z, t) = i \xi \mathcal{N} \hat{\sigma}_{12}(z, t), \quad (19)$$

where \mathcal{N} is the atomic density. The Fourier transform of the quantum operator satisfy the following equation:

$$\frac{1}{k_p} \frac{\partial}{\partial z} \hat{a}(\omega) = \chi \hat{a}(\omega) + \hat{F}_a, \quad (20)$$

where the coupling light and the MW field are treated as classical fields while the weak probe light is quantized. The probe light is described by slowly varying quantum mechanical operators. \hbar is Planck's constant. $\Omega_c = \mu_{32} E_c / \hbar$ and $\Omega_{MW} = \mu_{43} E_{MW} / \hbar$ are the Rabi frequency of the coupling light and the MW field, respectively. ξ is the atom-probe coupling constant: $\xi = \mu_{21} \varepsilon / \hbar$, where μ_{ij} ($i, j = 1, 2, 3, 4$) is the transition dipole moment from state $|i\rangle$ to state $|j\rangle$ and $\varepsilon = \sqrt{\hbar \omega_p / 2 \epsilon_0 V}$ is the electric field of a single photon. V is the quantized volume, \hat{a} is the annihilation operator for probe field, and ϵ_0 is the permittivity in vacuum. $\Delta_c = \omega_{32} - \omega_c$, $\Delta_{MW} = \omega_{43} - \omega_{MW}$, and $\Delta_p = \omega_{21} - \omega_p$ are the single-photon detuning of coupling light, the MW field, and the probe light, respectively. The properties of the medium are described by the collective slowly varying operators $\sigma_{\mu\nu}(z, t) = 1/N_z \sum_{j=1}^{N_z} |\mu_j\rangle \langle \nu_j| e^{-i\Delta_p t + i k_p z}$, averaged over small layers denoted by their position z containing N_z atoms. k_p is the projection of the wave vector of the probe light on the z axis. To account for decay and dephasing because of spontaneous emission, collision, transit-time broadening, etc., the system is described using the Heisenberg-Langevin equations:

$$\frac{\partial}{\partial t} \hat{\sigma}_{\mu\nu} = \frac{i}{\hbar} [\hat{H}, \hat{\sigma}_{\mu\nu}] + \hat{D}_{\mu\nu} + \hat{F}_{\mu\nu}. \quad (17)$$

Here, the $\hat{D}_{\mu\nu}$ are the terms produced by decay and dephasing:

where k_p is the wave vector of the probe, χ is the susceptibility of the medium dressed by the coupling light and the MW field. $\hat{F}_a = \sum_{m=2,3,4} i \xi \mathcal{N} B_{1m} \hat{F}_{1m}$. The coefficients column $[B_{1m}]$ is

$$[B_{1m}] = \frac{1}{S} \times \begin{bmatrix} \Omega_{MW} \Omega_{MW}^* + 4\Gamma_{13} \Gamma_{14} \\ -2i\Omega_c \Gamma_{14} \\ -\Omega_c \Omega_{MW} \end{bmatrix}.$$

Here, $S = \Gamma_{12}(4\Gamma_{13} \Gamma_{14} + \Omega_{MW} \Omega_{MW}^*) + \Gamma_{14} \Omega_c \Omega_c^*$, with $\Gamma_{12} = i\Delta_p + \gamma_2/2$, $\Gamma_{13} = i(\Delta_p + \Delta_c) + \gamma_3/2$, $\Gamma_{14} = i\Delta + \gamma_4/2$, and $\Delta = \Delta_c + \Delta_{MW} + \Delta_p$. The formula for the

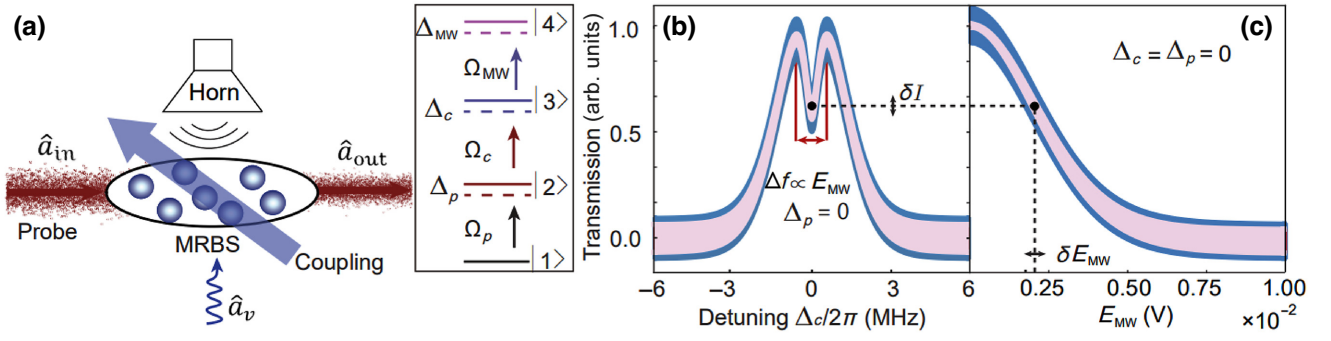


FIG. 3. (a) A schematic diagram for the RAEs. \hat{a}_v , vacuum field induced by the absorption measurement; Horn, microwave horn; MRBS, microwave-dressed Rydberg-atomic beam splitter. The inset shows an energy-level diagram of the RAEs. The subscripts p , c , and MW represent the probe, coupling, and the MW field, Δ_p , Δ_c , and Δ_{MW} are their single-photon detunings, and Ω_p , Ω_c , and Ω_{MW} indicate their Rabi frequencies. (b) The change in the transmission with the detuning of the coupling field. Here, Δf denotes the frequency distance between the two peaks and $\Delta f \propto E_{MW}$. (c) The relation between the transmission and the amplitude of the field E_{MW} when $\Delta_p = \Delta_c = 0$. The intensity fluctuation represented by the violet shade in (b) and (c) limits the sensitivity in measuring the electric field E_{MW} to the shot-noise limit (blue) and the squeezed quantum noise (red).

susceptibility in Rydberg atoms can be expressed as

$$\chi = \frac{i\mathcal{N}|\mu_{21}|^2}{\epsilon_0\hbar} \frac{\Gamma_{13}\Gamma_{14} + \frac{\Omega_{MW}\Omega_{MW}^*}{4}}{\Gamma_{12}[\Gamma_{13}\Gamma_{14} + \frac{\Omega_{MW}\Omega_{MW}^*}{4}] + \frac{\Omega_c\Omega_c^*}{4}\Gamma_{14}}. \quad (21)$$

The formal integration of the quantum operator is

$$\hat{a}_{out} = e^{-(\epsilon+i\phi)}\hat{a}_{in} + \sqrt{1 - e^{-2(\epsilon+i\phi)}}\hat{a}_v, \quad (22)$$

where $\epsilon = -\text{Im}(\chi)k_p l$ is the absorption index, $\phi = -\text{Re}(\chi)k_p l$ is the dispersion index, and l is the length of the atomic medium. $\hat{a}_v(t) = \int d\tau \hat{F}_a(\tau) e^{i\tau} / \sqrt{1 - e^{-2(\epsilon+i\phi)t}}$. With $\gamma_2 \gg \gamma_3$ and $\gamma_2 \gg \gamma_4$ [15], it is easy to verify $\langle \hat{a}_v(t) \rangle = 0$, $\langle \hat{a}_v(t)\hat{a}_v(t') \rangle = 0$, $\langle \hat{a}_v^\dagger(t)\hat{a}_v^\dagger(t') \rangle = 0$, $\langle \hat{a}_v^\dagger(t)\hat{a}_v(t') \rangle = 0$, and $\langle \hat{a}_v(t)\hat{a}_v^\dagger(t') \rangle = \delta(t-t')$, with D_1 and D_2 (see details in the Appendix). The input-output relation is consistent with Eq. (2), which denotes an induction of vacuum field \hat{a}_v in the loss measurement.

From the above, we note that the transmission of the probe light is a function of the MW field E_{MW} . Obviously, the intensity fluctuation and slope simultaneously affect the sensitivity for measuring the MW field. At a position with a large slope, we can sensitively measure the MW field by observing the intensity of the transmitted probe light, as shown in Figs. 3(b) and 3(c).

IV. SENSITIVITY OPTIMIZATION OF ELECTROMETER

In this section, we will analyze the optimal operating point of the RAEs in the classical-light and squeezed-light schemes, respectively, and give their best sensitivity. As

we have described above, the maximal quantum enhancement of absorptive detection can be reached when $\epsilon \rightarrow 0$. However, the slope $|\partial\epsilon/\partial E_{MW}|$ from the coupling of the MW field through AT splitting at this point approaches zero and is therefore away from the effective application of quantum enhancement for MW-field measurement. In order to sensitively measure the weak MW field, it is essential to find an operating point with a large slope in the classical scheme, since the noise and slope jointly determine the sensitivity, as shown in Fig. 3(c). We employ a dressed MW field E_{MW}^0 the frequency of which is resonant with the Rydberg transitions. The dressed MW field causes the splitting of the transmitted peak, therefore engineering the transmission and the slope of the probe. We focus on the ability of the system to sense a very weak MW field δE_{MW} with a dressed MW field E_{MW}^0 ; here we define a MW field of $E_{MW} = E_{MW}^0 + \delta E_{MW}$. The sensitivity in measuring the δE_{MW} field depends on Δ_c and E_{MW}^0 .

In Figs. 4(a) and 4(b), we compare the performance in measuring the MW field of cold RAEs by the coherent-light- and squeezed-light-injection schemes, respectively. The sensitivity is plotted as a function of the detuning of the coupling light Δ_c and the strength of the dressed MW field E_{MW}^0 ; the optimal sensitivity is labeled with a white circle, where $\Delta_c = 0$ and $\Delta_p = 0$, and a small dressed MW field is applied. In order to reveal the difference between the quantum and classical strategies more clearly, the evolution of their sensitivity with the dressed MW field when $\Delta_c = 0$ is shown in Fig. 4(c). The employment of squeezed light can improve the sensitivity compared with classical light with different values of E_{MW} , as shown by the red and blue lines. In the case of squeezed light, the optimum sensitivity is $2.1 \times 10^{-11} \text{ V m}^{-1} \text{ Hz}^{-1/2}$ with a dressed field of $E_{MW}^0 = 1 \times 10^{-4} \text{ V}$, which gives $G_q = 3$

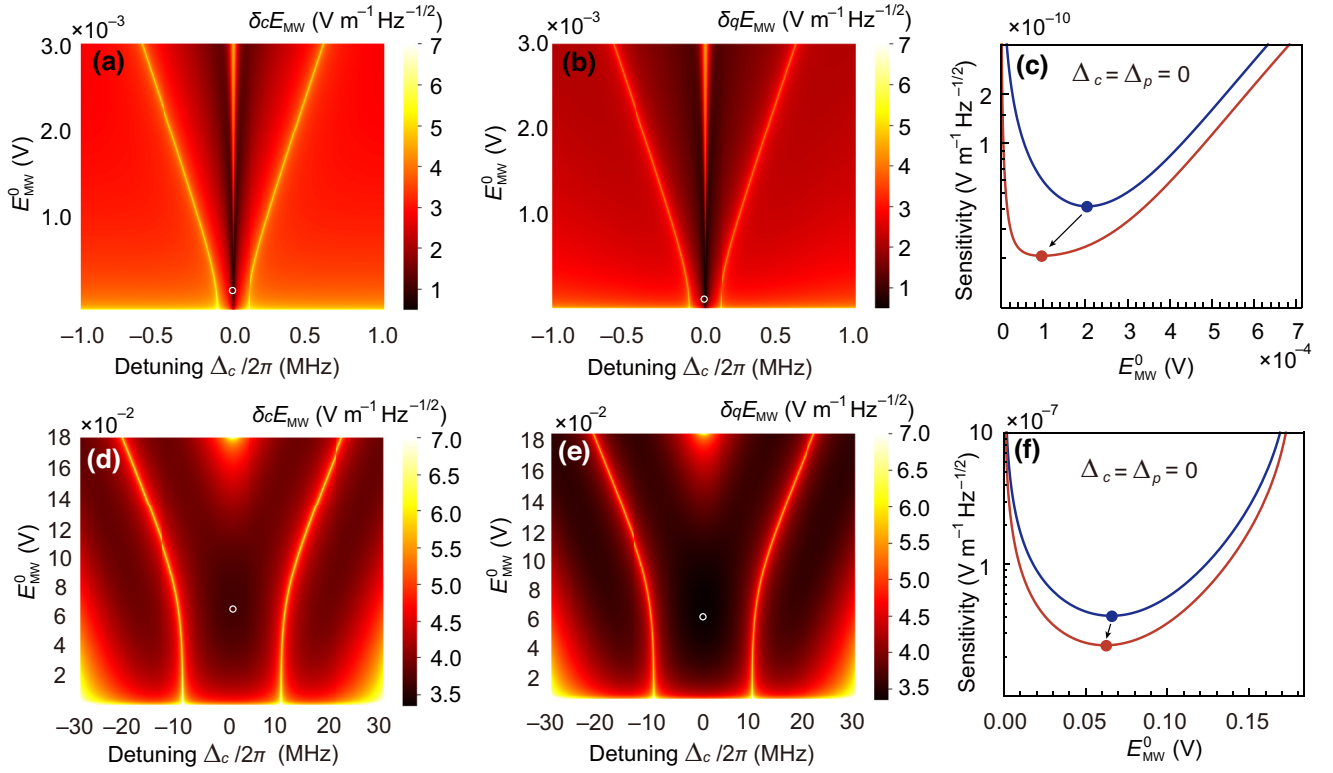


FIG. 4. The sensitivity with the detuning Δ_c and the amplitude E_{MW} of the MW field in the case of (a)–(c) cold atoms and (d)–(f) hot atoms. (a),(d) Coherent scheme. (b),(e) Squeezed-light scheme. (c),(f) The sensitivity change with the amplitude E_{MW} for $\Delta_c = \Delta_p = 0$. The blue red lines represent the sensitivities of classical-light injection and squeezed light with $Te^{-2\epsilon} = R$, respectively. The blue and red dots denote the optimal sensitivity of the classical light and squeezed light, respectively. The black line with an arrow indicates the quantum enhancement. Here, the interaction time $t = 1$ s and we set $\alpha = 10^7$, $r = 2.5$. The decay rates of the energy levels, $\gamma_1 = 0$, $\gamma_2 = 3.2889 \times 10^7$ s $^{-1}$, $\gamma_3 = 3.9423 \times 10^3$ s $^{-1}$, and $\gamma_4 = 2.5806 \times 10^3$ s $^{-1}$, are calculated based on the Cs-atom lifetime parameters. The atomic densities of the cold and hot atomic systems are $\mathcal{N} = 4.9 \times 10^{16}$ m $^{-3}$ and $\mathcal{N} = 4.9 \times 10^{19}$ m $^{-3}$, respectively.

compared with classical light according to Eq. (15), while the optimal sensitivity in the classical-light case is 4.1×10^{-11} V m $^{-1}$ Hz $^{-1/2}$ at $E_{MW}^0 = 2 \times 10^{-4}$ V. The noise of the squeezed light is extremely sensitive to the loss, which leads to an inconsistency of the optimal-sensitivity points compared with classical light. We should note that the optimal point is not operated when the probe field is fully transmitted, because the quantum light is slightly absorbed, which is the main loss in our scheme. A suitable photon number $\alpha = 10^7$ [25] is chosen here to optimize the sensitivity of the RAEs by balancing the collision rates and the power broadening due to the increase of the laser power.

Since thermal motion of the atoms is inevitable, Doppler broadening should be considered when the system runs at room temperature. Next, we discuss the influence of the Doppler effect and give the optimal sensitivity in the case of hot atomic vapor. The atoms in the vapor satisfy the Maxwell-Boltzmann distribution of velocities,

$$f(v) = \sqrt{\frac{M}{2\pi k_B T}} e^{-\frac{Mv^2}{2k_B T}}, \quad (23)$$

where M is the mass of the atom, k_B is the Boltzmann constant, v is the velocity, and T is the temperature. The atoms move with different velocities, leading to a revision of the detuning:

$$\Delta'_c = \Delta_c - \kappa_c f(v), \quad \Delta'_p = \Delta_p + \kappa_p f(v). \quad (24)$$

Here, κ_c and κ_p are the wave number of the probe and the coupling light, respectively. By performing velocity integration, we can obtain the susceptibility under hot-atom conditions, $\chi(v)_{\text{hot}} = \int_{-\infty}^{+\infty} \chi'(v) f(v) dv$. Here, $\chi'(v)$ represents the susceptibility when replacing Δ_c and Δ_p in Eq. (21) with Δ'_c and Δ'_p .

Figures 4(d)–4(f) give the relationship between the detuning Δ_c , the amplitude E_{MW} of the MW field, and the sensitivity of classical-light [Fig. 4(d)] and squeezed-light [Fig. 4(e)] injection in the case of hot atoms. For hot atoms, the trend of the sensitivity is consistent with that of cold atoms. Although the number of hot atoms increases by 3 orders of magnitude relative to the number of cold atoms, due to the distribution of the velocities, broadening the

transmission spectrum leads to a smaller slope and greater absorption, which results in a smaller signal and a decrease in quantum enhancement, respectively. The overall variation leads to a worse sensitivity compared with cold atoms. We have fixed the detuning $\Delta_c = 0$, and changing the E_{MW}^0 , as shown in Fig. 4(f). The optimal sensitivity of the RAEs with the classical and squeezed-light injection is $4 \times 10^{-8} \text{ V m}^{-1} \text{ Hz}^{-1/2}$ and $2.4 \times 10^{-8} \text{ V m}^{-1} \text{ Hz}^{-1/2}$, respectively, at about $E_{\text{MW}}^0 = 6.5 \times 10^{-2} \text{ V}$.

V. CONCLUSIONS

In summary, we have investigated an absorptive-measurement scheme that beats the limitation of the PSN by employing squeezed light. The quantum enhancement increases linearly with the gain when there is no absorption and tends to saturates with the gain when absorption exists. Loss is the main limitation for the current strategy to fully utilize the injected quantum resource. Furthermore, we have studied the entanglement-assisted microwave electrometer in the Rydberg-atomic regime by employing squeezed light with the absorptive measurement scheme. The noise squeezing makes it possible to break the bottleneck in which the limited power of the sensing field restricts the sensitivity due to the laser-induced collision rates and power broadening in the atomic system. Our theoretical analysis shows that the quantum advantage in our strategy can possibly be maintained in absorptive sensors over a large range of MW-field amplitudes by optimally choosing the operating parameters of the VBS, the optical field, and the atomic vapor. Squeezed-light-assisted RAEs outperform the classical scenario when the atomic vapor is operated in both the cold and hot regimes.

Furthermore, we can consider the dispersion that changes the relative phase [26] of the input laser beam for quantum-enhanced MW-field sensing through a phase-sensitive process. The coherence time of the atoms is related to the power of the probe light. In our model, we consider the coherence time of the atoms to be the same for both the coherent-light and squeezed-light scenarios. Compared to classical light, squeezed light can achieve the same measurement sensitivity with fewer photons, resulting in a smaller power broadening, which means a longer coherence time. Therefore, taking this into account, the ultimate quantum enhancement can be further improved. We note that black-body radiation (BBR) might be an important factor limiting the sensitivity. At room temperature ($T=300 \text{ K}$), the thermal noise level corresponds to an effective field of $4.8 \times 10^{-8} \text{ V m}^{-1} \text{ Hz}^{-1/2}$ [27]. Our results demonstrate that the use of squeezed light enables better observation of BBR. In cold atomic systems, ($T = 100 \text{ } \mu\text{K}$), the intensity of BBR is extremely weak (below the order of $\text{fV cm}^{-1} \text{ Hz}^{-1/2}$); therefore the effect of BBR is negligible. In this work, we utilize squeezed light as

the probe light, while the coupling light remains classical, since the power of the coupling light is greater than that of the probe light. When the power of the coupling light is comparable to the power of the probe light, the quantum noise of the coupling light needs to be taken into consideration. Our research hopefully paves the way for a promising outlook for quantum light sources in the field of absorptive measurement and MW-field sensing in the future.

ACKNOWLEDGMENTS

We acknowledge financial support from the Innovation Program for Quantum Science and Technology (2021ZD0303200), the National Natural Science Foundation of China (Grants No. 12234014, No. 12204304, No. 12374331, No. 11904227, and No. 11654005), the Shanghai Municipal Science and Technology Major Project (Grant No. 2019SHZDZX01), the Fellowship of China Postdoctoral Science Foundation (Grants No. 2020TQ0193, No. 2021M702146, No. 2021M702150, No. 2021M702147, and No. 2022T150413), the Sailing Program of the Science and Technology Commission of Shanghai Municipality (Grant No. 19YF1421800), the Fundamental Research Funds for the Central Universities, and the National Key Research and Development Program of China (Grant No. 2016YFA0302001). W.Z. acknowledges additional support from the Shanghai Talent Program.

The authors declare that there are no conflicts of interest related to this paper.

APPENDIX A: STEADY STATE

In the zeroth-order perturbation expansion, in which \hat{a} goes to zero, the Heisenberg-Langevin equations for the $\hat{\sigma}_{11}$, $\hat{\sigma}_{22}$, $\hat{\sigma}_{33}$, $\hat{\sigma}_{44}$, $\hat{\sigma}_{23}$, $\hat{\sigma}_{32}$, $\hat{\sigma}_{24}$, $\hat{\sigma}_{42}$, $\hat{\sigma}_{34}$, and $\hat{\sigma}_{43}$ atomic operators are decoupled. The mean values of these operators are required for the next-order solution. We assume the coupling light and MW field to propagate without depletion, as we have verified numerically. Then, the subset of equations for the mean-value variables $\langle \hat{\sigma}_{11} \rangle$, $\langle \hat{\sigma}_{22} \rangle$, $\langle \hat{\sigma}_{33} \rangle$, $\langle \hat{\sigma}_{44} \rangle$, $\langle \hat{\sigma}_{23} \rangle$, $\langle \hat{\sigma}_{32} \rangle$, $\langle \hat{\sigma}_{24} \rangle$, $\langle \hat{\sigma}_{42} \rangle$, $\langle \hat{\sigma}_{34} \rangle$, and $\langle \hat{\sigma}_{43} \rangle$ to be solved in the steady state is written in matrix form as follows:

$$\left([I]_{9 \times 9} \frac{\partial}{\partial t} - [M_0] \right) [\Sigma_0] = [S_0], \quad (\text{A1})$$

where $[I]_{9 \times 9}$ is the 9×9 identity matrix,

$$M_0 = \begin{bmatrix} -\gamma_4 & \gamma_2 - \gamma_4 & \gamma_3 - \gamma_4 & 0 & 0 & 0 & 0 & 0 & 0 \\ 0 & -\gamma_2 & 0 & \frac{-i\Omega_c}{2} & \frac{i\Omega_c}{2} & 0 & 0 & 0 & 0 \\ 0 & 0 & -\gamma_3 & \frac{i\Omega_c}{2} & \frac{-i\Omega_c}{2} & 0 & 0 & \frac{\Omega_{MW}}{2} & \frac{-\Omega_{MW}}{2} \\ 0 & \frac{-i\Omega_c}{2} & \frac{i\Omega_c}{2} & \frac{i2\Delta_c - \gamma_3 - \gamma_2}{2} & 0 & \frac{-i\Omega_{MW}}{2} & 0 & 0 & 0 \\ 0 & \frac{i\Omega_c}{2} & \frac{-i\Omega_c}{2} & 0 & \frac{-i2\Delta_c - \gamma_3 - \gamma_2}{2} & 0 & \frac{i\Omega_{MW}}{2} & 0 & 0 \\ 0 & 0 & 0 & \frac{-i\Omega_{MW}}{2} & 0 & \frac{-\beta_1}{2} & 0 & \frac{i\Omega_c}{2} & 0 \\ 0 & 0 & 0 & 0 & \frac{i\Omega_{MW}}{2} & 0 & \frac{-\beta_2}{2} & 0 & \frac{-i\Omega_c}{2} \\ \frac{-i\Omega_{MW}}{2} & \frac{-i\Omega_{MW}}{2} & -i\Omega_{MW} & 0 & 0 & \frac{i\Omega_c}{2} & 0 & \frac{-\gamma_3 - \gamma_4 - i2\Delta_{MW}}{2} & 0 \\ \frac{i\Omega_{MW}}{2} & \frac{i\Omega_{MW}}{2} & i\Omega_{MW} & 0 & 0 & 0 & \frac{-i\Omega_c}{2} & 0 & \frac{-\gamma_3 - \gamma_4 + i2\Delta_{MW}}{2} \end{bmatrix}, \quad (A2)$$

$$[\hat{\Sigma}_0] = \begin{bmatrix} \hat{\sigma}_{11} \\ \hat{\sigma}_{22} \\ \hat{\sigma}_{33} \\ \hat{\sigma}_{23} \\ \hat{\sigma}_{32} \\ \hat{\sigma}_{24} \\ \hat{\sigma}_{42} \\ \hat{\sigma}_{34} \\ \hat{\sigma}_{43} \end{bmatrix}, \quad [S_0] = \begin{bmatrix} \gamma_4 \\ 0 \\ 0 \\ 0 \\ 0 \\ 0 \\ 0 \\ \frac{i\Omega_{MW}}{2} \\ \frac{-i\Omega_{MW}}{2} \end{bmatrix}. \quad (A3)$$

where $\beta_1 = \gamma_2 + \gamma_4 + i2\Delta_c + i2\Delta_{MW}$ and $\beta_2 = \gamma_2 + \gamma_4 - i2\Delta_c - i2\Delta_{MW}$. The steady-state solution of Eq. (A1) is

$$[\langle \Sigma_0 \rangle] = [M_0]^{-1}[S_0]. \quad (A4)$$

APPENDIX B: ATOMIC HEISENBERG-LANGEVIN EQUATIONS

The first-order solution for the three coherences σ_{12} , σ_{13} , and σ_{14} is determined by the following matrix equation:

$$\left([I]_{3 \times 3} \frac{\partial}{\partial t} - [M_1] \right) [\hat{\Sigma}_1] = [S_1] \hat{a} + [\hat{F}_1], \quad (B1)$$

with

$$M_1 = \begin{bmatrix} \frac{-\gamma_2}{2} - i\Delta_p & \frac{-i\Omega_c}{2} & 0 \\ \frac{-i\Omega_c}{2} & \frac{-\gamma_3}{2} - i(\Delta_p + \Delta_c) & \frac{-i\Omega_{MW}}{2} \\ 0 & \frac{-i\Omega_{MW}}{2} & \frac{-\gamma_4}{2} - i\Delta \end{bmatrix}, \quad (B2)$$

$$[\hat{\Sigma}_1] = \begin{bmatrix} \hat{\sigma}_{12} \\ \hat{\sigma}_{13} \\ \hat{\sigma}_{14} \end{bmatrix}, \quad [S_1] = \xi \begin{bmatrix} i\langle \hat{\sigma}_{22} - \hat{\sigma}_{11} \rangle \\ i\langle \hat{\sigma}_{23} \rangle \\ i\langle \hat{\sigma}_{24} \rangle \end{bmatrix}, \quad [\hat{F}_1] = \begin{bmatrix} \hat{F}_{12} \\ \hat{F}_{13} \\ \hat{F}_{14} \end{bmatrix}. \quad (B3)$$

Here, $[I]_{3 \times 3}$ is the 3×3 identity matrix. The annihilation operators are denoted by \hat{a} and $\Delta = \Delta_p + \Delta_c + \Delta_{MW}$. The Langevin atomic forces $[\hat{F}]$ are characterized by the matrix of their diffusion coefficients, $[D_1] + [D_2]$, defined as

$$[D_1]2\delta(t-t')\delta(z-z') = \langle [\hat{F}_{1(z,t)}]^\dagger [\hat{F}_{1(z,t')}] \rangle, \quad (B4)$$

$$[D_2]2\delta(t-t')\delta(z-z') = \langle [\hat{F}_{1(z,t')}]^\dagger [\hat{F}_{1(z,t)}] \rangle. \quad (B5)$$

Langevin diffusion coefficients for the operators can be calculated using the generalized Einstein relation [28]. The $[D_1]$ and $[D_2]$ diffusion matrices are given by

$$D_1 = \begin{bmatrix} \gamma_2 & 0 & 0 \\ 0 & \gamma_3 & 0 \\ 0 & 0 & \gamma_4 \end{bmatrix}, \quad D_2 = \begin{bmatrix} 0 & 0 & 0 \\ 0 & 0 & 0 \\ 0 & 0 & 0 \end{bmatrix}. \quad (B6)$$

By linearizing Eq. (B1), we derive, for the mean values,

$$[\langle \hat{\Sigma}_1 \rangle] = -[M_1]^{-1}[S_1][\langle \hat{a} \rangle] \quad (\text{B7})$$

and for the Fourier-transformed quantum fluctuations,

$$\begin{aligned} [\delta \hat{\Sigma}_1] = & -([M_1] + i\omega[I]_{3 \times 3})^{-1}[S_1][\delta \hat{a}] \\ & - ([M_1] + i\omega[I]_{3 \times 3})^{-1}[\hat{F}_1]. \end{aligned} \quad (\text{B8})$$

Here, ω is the analysis frequency.

APPENDIX C: SELECTION OF COUPLING INTENSITY

When the coupling-light intensity is relatively low, it corresponds to a small signal. However, when the coupling-light intensity is relatively high, the two peaks of the AT splitting completely separate, which results in the point $\Delta_c = \Delta_p = 0$ being completely insensitive to the MW field. Therefore, we choose an intermediate value of $\Omega_c = 2 \times 10^7$ Hz in the final measurement [8,17].

-
- [1] U. L. Rohde, J. C. Whitaker, and H. Zehn *Communications Receivers: Principles and Design* (McGraw-Hill Education, 2017), 4th ed, <https://www.accessengineeringlibrary.com/content/book/9780071843331>.
- [2] D. H. Meyer, K. C. Cox, F. K. Fatemi, and P. D. Kunz, Digital communication with Rydberg atoms and amplitude-modulated MW fields, *Appl. Phys. Lett.* **112**, 211108 (2018).
- [3] A. K. Robinson, N. Prajapati, D. Senic, and M. T. Simons, Determining the angle-of-arrival of a radio-frequency source with a Rydberg atom-based sensor, *Appl. Phys. Lett.* **118**, 114001 (2021).
- [4] Y. Kim, J. S. Kimball, K. C. McDonald, and J. Glassy, Developing a global data record of daily landscape freeze/thaw status using satellite passive microwave remote sensing, *IEEE Trans. Geosci. Remote* **49**, 949 (2010).
- [5] A. N. Reznik and N. V. Yurasova, Electrodynamics of microwave near-field probing: Application to medical diagnostics, *J. Appl. Phys.* **98**, 114701 (2005).
- [6] N. K. Nikolova, Microwave imaging for breast cancer, *IEEE Microw. Mag.* **12**, 78 (2011).
- [7] M. Guardiola, S. Buitrago, G. Fernández-Esparrach, J. M. O’Callaghan, J. Romeu, M. Cuatrecasas, H. Córdova, M. Á. G. Ballester, and O. Camara, Dielectric properties of colon polyps, cancer, and normal mucosa: Ex vivo measurements from 0.5 to 20 GHz, *Med. Phys.* **45**, 3768 (2018).
- [8] J. A. Sedlacek, A. Schwettmann, H. Kübler, R. Löw, T. Pfau, and J. P. Shaffer, Microwave electrometry with Rydberg atoms in a vapour cell using bright atomic resonances, *Nat. Phys.* **8**, 819 (2012).
- [9] J. A. Sedlacek, A. Schwettmann, H. Kübler, and J. P. Shaffer, Atom-based vector microwave electrometry using rubidium Rydberg atoms in a vapor cell, *Phys. Rev. Lett.* **111**, 063001 (2013).
- [10] Z. K. Liu, L. H. Zhang, B. Liu, Z. Y. Zhang, G. C. Guo, D. S. Ding, and B. S. Shi, Deep learning enhanced Rydberg multifrequency microwave recognition, *Nat. Commun.* **13**, 1997 (2022).
- [11] D. S. Ding, Z. K. Liu, B. S. Shi, G. C. Guo, K. Mølme, and C. S. Adams, Enhanced metrology at the critical point of a many-body Rydberg atomic system, *Nat. Phys.* **18**, 1447 (2022).
- [12] M. Fleischhauer, A. Imamoglu, and J. P. Marangos, Electromagnetically induced transparency: Optics in coherent media, *Rev. Mod. Phys.* **77**, 633 (2005).
- [13] S. H. Autler and C. H. Townes, Stark effect in rapidly varying fields, *Phys. Rev.* **100**, 703 (1955).
- [14] T. Gallagher, *Rydberg Atoms* (Cambridge University, 2005), https://books.google.com.hk/books/about/Rydberg_Atoms.html?id=8JIpEhHWT-cC&redir_esc=y.
- [15] M. Jing, Y. Hu, J. Ma, H. Zhang, L. Zhang, L. Xiao, and S. Jia, Atomic superheterodyne receiver based on microwave-dressed Rydberg spectroscopy, *Nat. Phys.* **16**, 911 (2020).
- [16] S. Kumar, H. Fan, H. Kübler, J. Sheng, and J. P. Shaffer, Atom-based sensing of weak radio frequency electric fields using homodyne readout, *Sci. Rep.* **7**, 1 (2017).
- [17] S. Kumar, H. Fan, H. Kübler, A. J. Jahangiri, and J. P. Shaffer, Rydberg-atom based radio-frequency electrometry using frequency modulation spectroscopy in room temperature vapor cells, *Opt. Express* **25**, 8625 (2017).
- [18] X. Guo, C. R. Breum, J. Borregaard, S. Izumi, M. V. Larsen, T. Gehring, M. Christandl, J. S. Neergaard-Nielsen, and U. L. Andersen, Distributed quantum sensing in a continuous-variable entangled network, *Nat. Phys.* **16**, 281 (2020).
- [19] V. Giovannetti, S. Lloyd, and L. Maccone, Advances in quantum metrology, *Nat. Photonics* **5**, 222 (2011).
- [20] M. A. Taylor and W. P. Bowen, Quantum metrology and its application in biology, *Phys. Rep.* **615**, 1 (2016).
- [21] R. Schnabel, Squeezed states of light and their applications in laser interferometers, *Phys. Rep.* **684**, 1 (2017).
- [22] F. Wolfgramm, A. Cere, F. A. Beduini, A. Predojević, M. Koschorreck, and M. W. Mitchell, Squeezed-light optical magnetometry, *Phys. Rev. Lett.* **105**, 053601 (2010).
- [23] P. M. Anisimov, G. M. Raterman, A. Chiruvelli, W. N. Plick, S. D. Huver, H. Lee, and J. P. Dowling, Quantum metrology with two-mode squeezed vacuum: Parity detection beats the Heisenberg limit, *Phys. Rev. Lett.* **104**, 103602 (2010).
- [24] W. Du, J. Kong, G. Bao, P. Yang, J. Jia, S. Ming, C.-H. Yuan, J. F. Chen, Z. Y. Ou, M. W. Mitchell, and W. Zhang, SU(2)-in-SU(1, 1) nested interferometer for high sensitivity, loss-tolerant quantum metrology, *Phys. Rev. Lett.* **128**, 033601 (2022).
- [25] J. P. Shaffer and H. Kübler, A read-out enhancement for microwave electric field sensing with Rydberg atoms, *Proc. SPIE* **10674**, 106740 (2018).
- [26] W. Yang, M. Jing, H. Zhang, L. Zhang, L. Xiao, and S. Jia, Enhancing the sensitivity of atom-based microwave-field electrometry using a Mach-Zehnder interferometer, *Phys. Rev. Appl.* **19**, 064021 (2023).
- [27] S. Borówka, U. Pylypenko, M. Mazelanik, and M. Parniak, Continuous wideband microwave-to-optical converter based on room-temperature Rydberg atoms, Preprint [ArXiv:2302.08380](https://arxiv.org/abs/2302.08380) (2023).
- [28] L. Davidovich, Sub-Poissonian processes in quantum optics, *Rev. Mod. Phys.* **68**, 127 (1996).